3D Plant Cell Architecture of Arabidopsis thaliana (Brassicaceae) Using Focused Ion Beam–Scanning Electron Microscopy

Source: Applications in Plant Sciences, 2(6)

Published By: Botanical Society of America

URL: https://doi.org/10.3732/apps.1300090

Applications in Plant Sciences

Applications in Plant Sciences 2014 2(6): 1300090

Application Article

3D Plant cell architecture of *Arabidopsis thaliana* (Brassicaceae) using focused ion beam–scanning electron microscopy[1]

Bhawana[2], Joyce L. Miller[3], and A. Bruce Cahoon[2,4]

[2]Molecular Biosciences Program, Middle Tennessee State University, Murfreesboro, Tennessee 37132 USA; and [3]MTSU Interdisciplinary Microanalysis and Imaging Center, Middle Tennessee State University, Murfreesboro, Tennessee 37132 USA

- *Premise of the study:* Focused ion beam–scanning electron microscopy (FIB-SEM) combines the ability to sequentially mill the sample surface and obtain SEM images that can be used to create 3D renderings with micron-level resolution. We have applied FIB-SEM to study *Arabidopsis* cell architecture. The goal was to determine the efficacy of this technique in plant tissue and cellular studies and to demonstrate its usefulness in studying cell and organelle architecture and distribution.
- *Methods:* Seed aleurone, leaf mesophyll, stem cortex, root cortex, and petal lamina from *Arabidopsis* were fixed and embedded for electron microscopy using protocols developed for animal tissues and modified for use with plant cells. Each sample was sectioned using the FIB and imaged with SEM. These serial images were assembled to produce 3D renderings of each cell type.
- *Results:* Organelles such as nuclei and chloroplasts were easily identifiable, and other structures such as endoplasmic reticula, lipid bodies, and starch grains were distinguishable in each tissue.
- *Discussion:* The application of FIB-SEM produced 3D renderings of five plant cell types and offered unique views of their shapes and internal content. These results demonstrate the usefulness of FIB-SEM for organelle distribution and cell architecture studies.

Key words: *Arabidopsis thaliana*; cell architecture; FIB-SEM; plant cell tomography.

There are several microscopy methods available to obtain intra- or subcellular structural information (Micheva and Smith, 2007; Helmstaedter et al., 2008; Lehrer, 2009; Wei et al., 2012). One of these techniques, focused ion beam–scanning electron microscopy (FIB-SEM), uses two beams: (1) a focused gallium ion beam and (2) an electron beam with secondary electron detector. The gallium beam can be used for imaging, can mill an area of interest to serially expose surfaces to reveal tissue and cell features, or can be used to produce high-quality sections of a sample for transmission electron microscopy (TEM) studies. The SEM beam can visualize an area of interest similar to conventional SEM. When combined, they enable a microscopist to section and visualize a sample with the same apparatus (Tanaka and Mitsushima, 1984; Heymann et al., 2006; Marko et al., 2007; Drobne et al., 2008; Knott et al., 2008; De Winter et al., 2009; Merchán-Pérez et al., 2009; Schneider et al., 2010; Bushby et al., 2011; Wei et al., 2012). This technique has been used in material science for decades (Sugiyama and Sigesato, 2004; Giannuzzi, 2005; Giannuzzi et al., 2005) but has recently been gaining wider use on biological tissues and is proving to be a powerful technology for creating 3D reconstructions of whole cells (Merchán-Pérez et al., 2009; Bushby et al., 2011; Wei et al., 2012). In terms of cost, FIB-SEM requires a dedicated apparatus that would require an investment comparable to a transmission electron microscope or access to a facility with an existing apparatus. The advantages of FIB-SEM over TEM tomography are (1) the ease of sectioning and image acquisition and (2) the chance of error during image realignment is minimized because serial images are acquired from a stationary block face.

FIB-SEM has been used on biological tissues in two ways: (1) a sample may be embedded, sectioned, and imaged using the FIB-SEM apparatus (Heymann et al., 2006); or (2) in some cases, the FIB capability is used to produce high-quality sections for TEM imaging (Wei et al., 2012). FIB-SEM has, to date, been used to produce three-dimensional renderings of animal cells (Bushby et al., 2011), microorganisms (Heymann et al., 2006; Wei et al., 2012), starch granules in plant cells (Crumpton-Taylor et al., 2012), and pollen cells (House and Balkwill, 2013).

Our objective for this study was to modify and apply existing FIB-SEM protocols developed for animal tissues to produce three-dimensional renderings of five tissues from *Arabidopsis thaliana* (L.) Heynh. (root cortex, shoot cortex, seed aleurone, leaf mesophyll, and flower petal lamina). We found that several modifications were necessary to achieve images of plant cells with FIB-SEM and that cells with dense cytoplasm (i.e., seed

[1]Manuscript received 26 November 2013; revision accepted 25 April 2014.

The authors thank Middle Tennessee State University's Interdisciplinary Microanalysis and Imaging Center for donated time on the FIB-SEM apparatus, the Molecular Biosciences Program and the School of Graduate Studies for project support, and two anonymous reviewers and the *APPS* editorial team for helpful comments and suggestions.

[4]Author for correspondence: Aubrey.Cahoon@mtsu.edu

doi:10.3732/apps.1300090

aleurone and root cortex cells) yielded the best results. We were able to easily identify subcellular architecture and organelles in all tissue types.

MATERIALS AND METHODS

Plant tissue and growth conditions—*Arabidopsis thaliana* was chosen for this study due to its small size, rapid growth cycle, and importance as a model plant system. Tissues were chosen in an attempt to survey a range of cellular content.

Root cortex tissues were obtained from 7–10-d-old seedlings grown on filter paper saturated with 1/2× Murashige and Skoog medium (Murashige and Skoog, 1962). Dry seeds were used as a source of aleurone tissue. Leaf mesophyll, stem cortex, and petal lamina were obtained from 4–6-wk-old plants grown in potting soil at room temperature under fluorescent lights set on a 16 h light/8 h dark cycle.

Tissue fixation and preparation for FIB-SEM—A FIB-SEM protocol developed for animal tissues (Bushby et al., 2011) was the primary source for our methodology, with modifications based on Mikuła et al. (2004). FIB-SEM protocols for animal tissues have several modifications to the conventional fixation used in SEM or TEM methods, including en bloc staining using uranyl acetate (Heymann et al., 2006; Merchán-Pérez et al., 2009; Wei et al., 2012), prefixation in paraformaldehyde, and use of potassium ferricyanide and/or tannic acid to enhance the contrast (Knott et al., 2008, 2011; Armer et al., 2009; De Winter et al., 2009; Hekking et al., 2009; Bushby et al., 2011; Wei et al., 2012).

Fresh tissue was cut into ~1-mm square or block portions and initially fixed in 2–3 mL of 2.5% glutaraldehyde (v/v) and 2.0% paraformaldehyde (w/v) in pH 7.3 0.1 M sodium cacodylate buffer for 2 h on a rotator. The primary fixative was removed, and the tissue samples were washed 2 × 10 min in 0.1 M sodium cacodylate buffer. Tissues were immersed in 2–3 mL of secondary fixative (1% osmium tetroxide [v/v], 1.5% potassium ferricyanide [w/v], in 0.1 M sodium cacodylate buffer) at room temperature for 2 h. The secondary fixative was removed, and tissues were washed 3 × 10 min with 0.1 M sodium cacodylate buffer. Buffer was replaced with 1% tannic acid (w/v) for 1 h and then removed by immersion in distilled water 3 × 10 min. Tissues were dehydrated by immersion in 30, 50, 70, 95, and 3 × 100% ethanol, for 10 min each, followed by 2 × 10 min in 100% propylene oxide (PO) (v/v). Subsequently, the tissues were immersed in 3 : 1 PO : Epon+Spurr for 1 h, 1 : 1 PO : Epon+Spurr for 1 h, 1 : 3 PO : Epon+Spurr overnight at room temperature, then 100% Epon+Spurr for 24 h (Mikuła et al., 2004).

Fixed specimens were transferred into BEEM capsules (Ted Pella Inc., Redding, California, USA), oriented at the tip of the capsules, covered with 100% Epon+Spurr, and cured at 60°C for 24 h. The pyramidal ends of the plastic blocks were trimmed with a glass knife until tissue was reached. The area around the tissue was trimmed to form a trapezoid-shape measuring 0.5 mm × 1 mm (length × width). Each plastic block was immobilized with a vise, and a 4-mm portion containing the fixed tissue was removed using a fine hacksaw, forming a pyramid. The 4-mm pyramid was glued to a 12.5-mm aluminum SEM stub, using PELCO carbon tabs (Ted Pella Inc.), such that the imaging surface (the trapezoid) was horizontal to the stub surface. Each pyramid was coated with carbon glue excluding the trapezoidal surface. Finally, the pyramid was coated with a 200-nm layer of gold palladium using a Hummer 6.2 Sputtering Apparatus (Ladd Research Industries, Williston, Vermont, USA).

FIB-SEM—The gold palladium–coated sample was placed on the specimen stage of the FIB-SEM apparatus and secured with the sample facing toward the outer edge of the vacuum chamber and the chamber pumped to high vacuum. When the SEM electron beam was engaged, the area of interest was identified using the secondary electron detector in a wide field. Next, the FIB high voltage and emission current were turned on and the FIB window opened. Sample working distance was set to 9 mm and the stage tilted to 55°. FIB and SEM pictures were aligned using the FIB-SEM intersection (setting the eucentric position of the stage), and the magnification was set between 2500× and 3000×. A platinum layer (20 µm × 20 µm × 0.25 µm [length × width × height]) was deposited on the area of interest. For milling, the ion beam current was initially set to 1000 pA but optimal beam current varied and was manually adjusted sample to sample. The regular cross-section feature and ion beam were used to mill a trench (FIB coarse trench milling) 20 µm × 20 µm × 10 µm to expose the targeted area. Fine milling and the polishing feature were used to remove debris or imperfections from the front face of the platinum-coated area (targeted area). The block face was automatically or manually sliced using the FIB slicing + SEM image acquisition feature, with a thickness of 100 nm for each slice and 10 ns/slice dwell time.

Image processing—Images were processed using ImageJ (Schneider et al., 2012). Briefly, the area of interest was selected within the image frame and cropped. Brightness and/or contrast were adjusted and the processed images saved in TIFF format. ImageJ 3D viewer was used to compile the stack into a three-dimensional rendering, make orthogonal slices or 3D rotations, or save images in .avi format to be viewed as a movie.

RESULTS

Five different tissues were explored using FIB-SEM. Areas of interest included seed aleurone (Fig. 1a), stem cortex (Fig. 1d), root cortex (Fig. 1g), leaf mesophyll (Fig. 1j), and petal mesophyll (Fig. 1m). A 20 × 20 × 0.25-µm platinum layer was placed on each area of interest (Fig. 1b, e, h, k, n) to protect it from burning (or destruction) by the FIB beam as well as to provide a leveled surface for even slicing. A trench was milled around each platinum layer to expose the targeted area (block face) for sectioning and imaging (Fig. 1c, f, i, l, o).

Automated serial sectioning and imaging of seed aleurone cells provided 90 micrographs by serially removing 100-nm sections from the block face. Some manual images were also collected (Fig. 2a–c). Automated images were assembled to obtain a three-dimensional reconstruction, 360° orthogonal rotation (Figs. 3a, 4a; Videos 1a, 2a), and a three-dimensional false-colored volume rendering of the tissue (Fig. 5a).

Stem cortex cells adjacent to the epidermis and extending toward the vascular bundle were automatically sectioned and imaged to produce 141 micrographs. Several high-resolution manual images were also collected (Fig. 2d–f). Micrographs from serial sectioning were used to produce a three-dimensional reconstruction, 360° orthogonal rotation, and three-dimensional false-colored volume rendering for the stem tissue (Figs. 3b, 4b, 5b; Videos 1b, 2b).

Automated serial sectioning and imaging of root endodermis and cortex tissue yielded 88 micrographs. Manual images were also collected (Fig. 2g–i). Sections were assembled to produce a three-dimensional reconstruction (Fig. 3c, Video 1c), 360° orthogonal rotation (Fig. 4c, Video 2c), and three-dimensional false-colored volume rendering of the tissue (Fig. 5c).

Leaf mesophyll cells were automatically sectioned and imaged to yield 141 micrographs. Manual images were also collected (Fig. 2j–l). Serial sections were used to produce a three-dimensional reconstruction, 360° orthogonal rotation, and three-dimensional false-colored volume rendering of the tissue (Figs. 3d, 4d, 5d; Videos 1d, 2d).

Petal mesophyll cells were automatically sectioned and imaged to yield 142 micrographs. Manual images were also collected (Fig. 2 m–o). Sections were used to produce a three-dimensional reconstruction, 360° orthogonal rotation, and three-dimensional false-colored volume rendering of the tissue (Figs. 3e, 4e, 5e; Videos 1e, 2e).

DISCUSSION

Plant cell and tissue tomography has been possible for some time (Pellegrini, 1980), but recent improvements and accessibility in computational methodologies and image manipulation

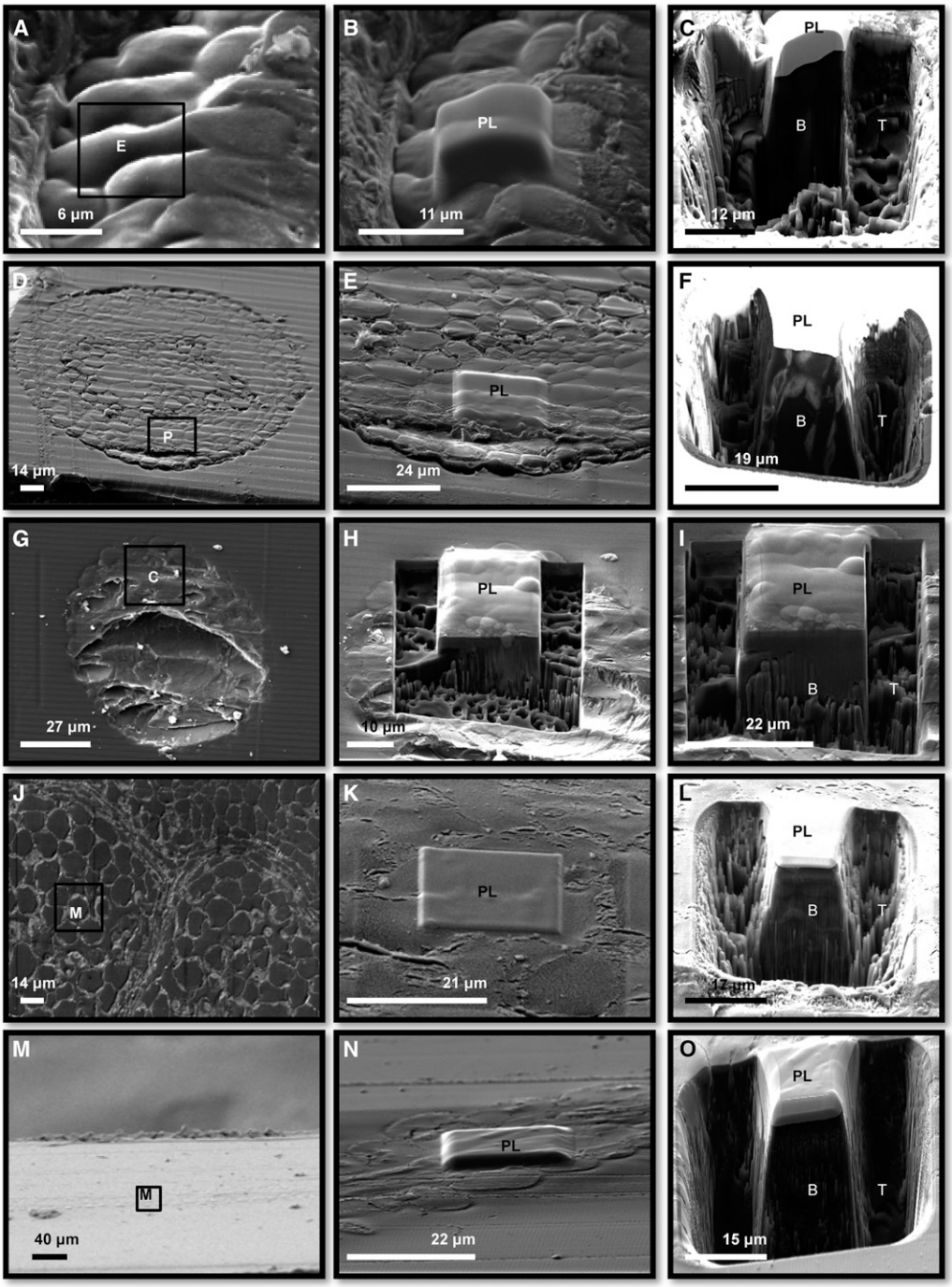

Fig. 1. Five *Arabidopsis* tissues prepared for FIB-SEM sectioning and imaging. Stages of the FIB-SEM process are demonstrated, including choosing an area of interest, depositing a platinum layer (PL), and milling to create a block for serial sectioning. Dry seeds were fixed, sliced, and imaged for aleurone visualization (a–c): (a) the endosperm cells (E)* of the aleurone area of interest viewed at a 55° angle; (b) a 250-nm platinum layer (PL) applied to the area of interest; (c) a U-shaped trench (T) was milled with the gallium ion beam around the area of interest to expose a block face (B) for sectioning and imaging. Stem tissue (d–f): (d) whole stem transverse section showing parenchymal (P)* cells; (e) a 250-nm platinum layer (PL) was placed on an area of interest across the cortex spanning from the first layer of parenchymal cells interior to the epidermis to the endodermis; (f) a milled trench (T) at the area of interest, the first parenchymal layer is visible on the block face (B). Root tissue (g–i): (g) cortex cells (C)* of a whole root transverse section from the elongation zone shown at a 0° angle; (h) a 250-nm platinum layer (PL) was placed on the cortex extending from the endodermis toward the epidermis, and a trench was partially milled, shown at a 55° angle; (i) the completed trench (T) showing an exposed block surface. Leaf tissue (j–l): (j) mesophyll cells (M)* were chosen as the area of interest, shown here at a 0° angle of a transverse section; (k) a 250-nm platinum layer (PL) on the area of interest (mesophyll cells); (l) a trench (T) was milled exposing the block face (B). White petals from fully opened flowers (m–o): (m) the faint outline of a petal transverse section is shown at a 55° angle (mesophyll cells [M]* were chosen for imaging); (n) a 250-nm platinum layer (PL) was placed on the area of interest; (o) a trench (T) was milled, exposing the block surface. Abbreviations: B = block face; C = cortex cells; E = endosperm cells; M = mesophyll cells; P = parenchymal cells; PL = platinum layer; T = trench. *Squares in a, d, g, j, and m represent the areas of interest for each tissue.

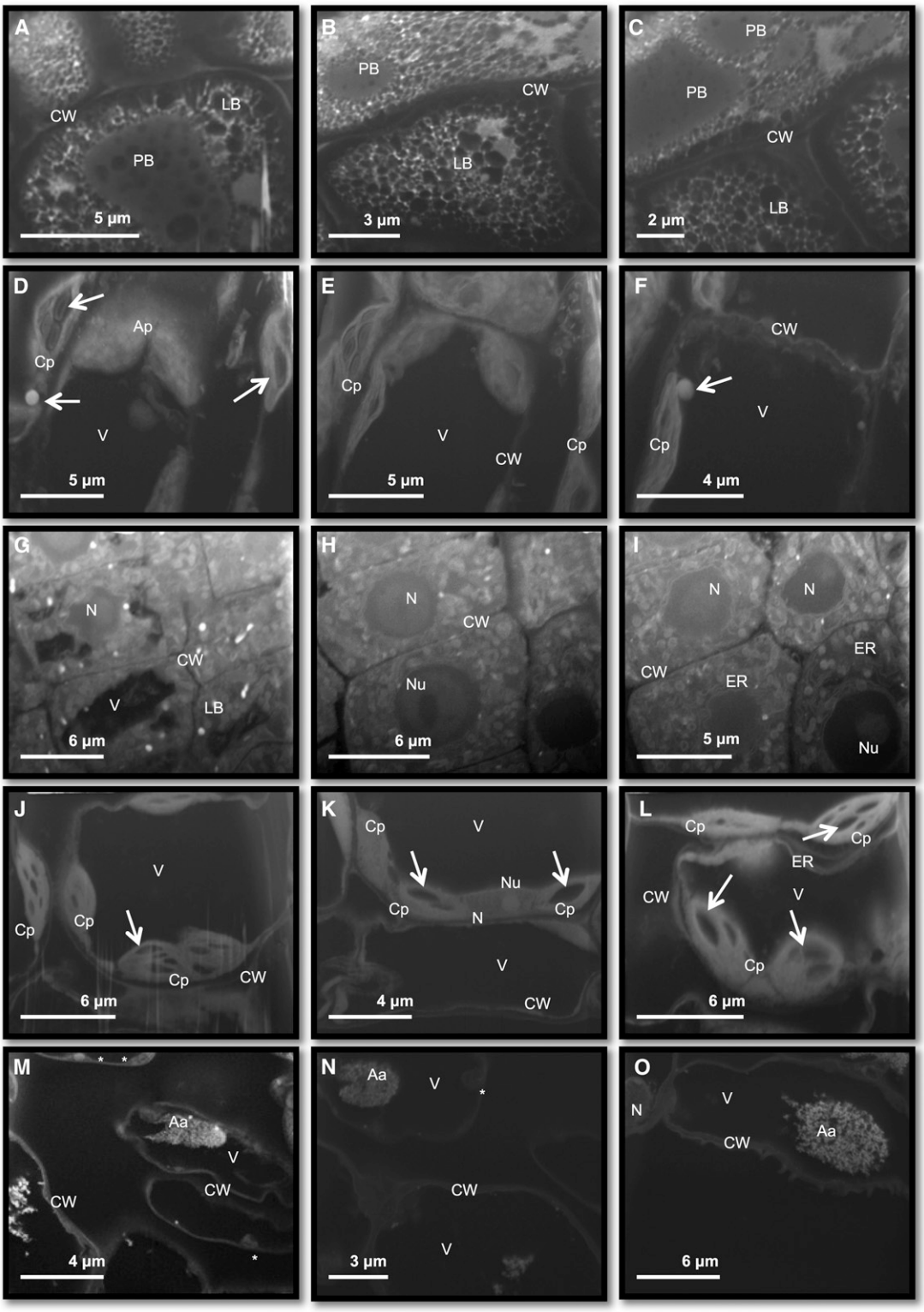

Fig. 2. High-resolution SEM micrographs from manual imaging. At least 40 images were collected from each cell type in this study. Three representative images from each cell type are shown and subcellular bodies labeled to demonstrate the resolution achieved. (a–c): Seed aleurone cells showing protein bodies (PB), lipid bodies (LB), and cell walls (CW). (d–f): Stem cortex cells showing chloroplasts (Cp), amyloplast (Ap), starch grains (arrows), cell wall (CW), and vacuoles (V). (g–i): Root cortex cells showing vacuole (V), nucleus (N), nucleolus (Nu), lipid bodies (LB), cell wall (CW), and endoplasmic reticulum (ER). (j–l): Leaf mesophyll cells showing chloroplasts (Cp) and internal membranous endoplasmic reticulum connections (ER). (m–o): Petal mesophyll cell showing nucleus (N), vacuoles (V) and amorphous aggregate (Aa), cell wall (CW), and some organelles (*) with details below the lower limit of the resolution of this technique. Abbreviations: Aa = amorphous aggregrate; Ap = amyloplast; Cp = chloroplast; CW = cell wall; ER = endoplasmic reticulum; LB = lipid body; N = nucleus; Nu = nucleolus; PB = protein body; V = vacuole.

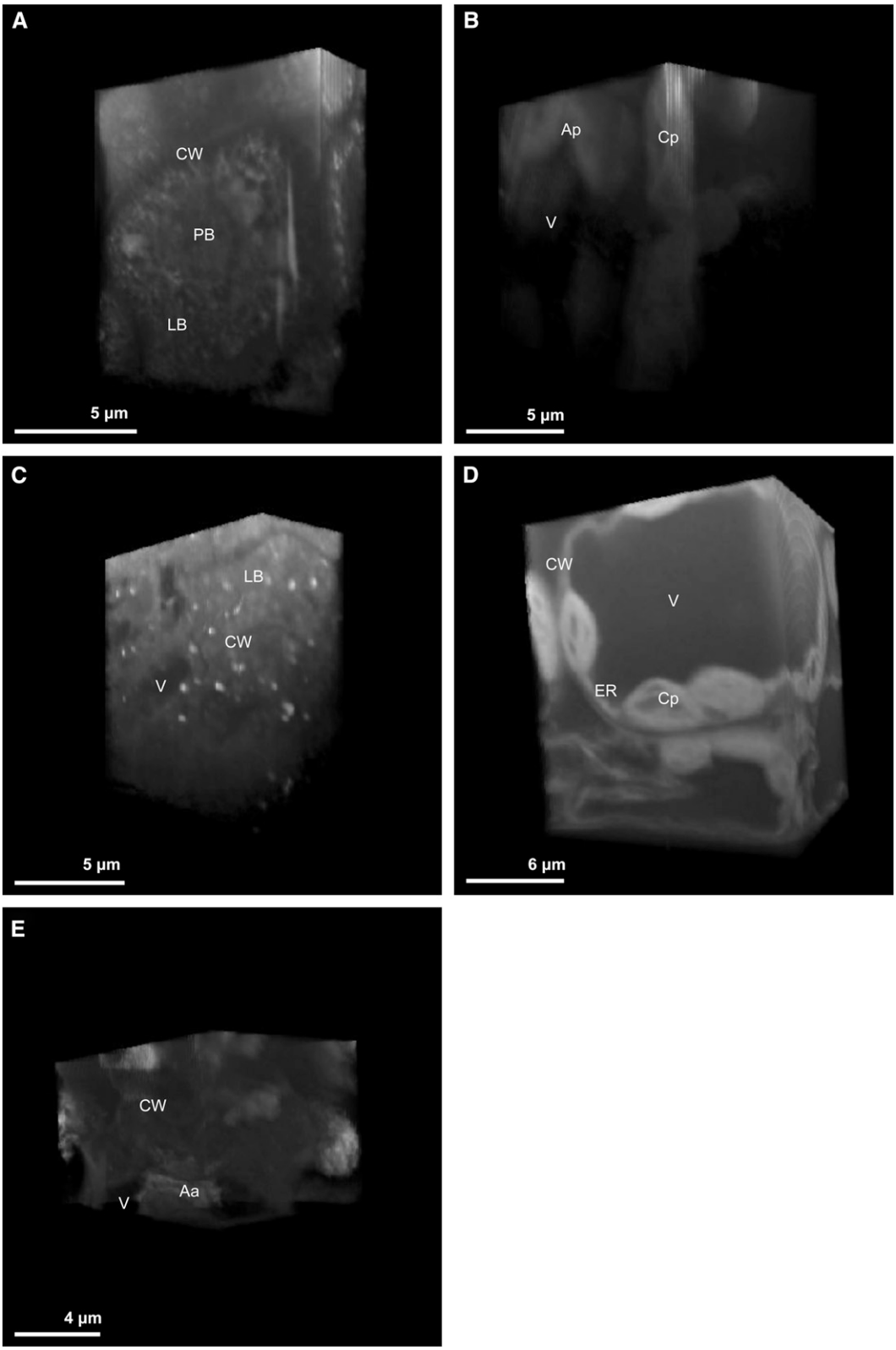

Fig. 3. 3D renderings of the imaged areas of interest from the five tissues. Serial images were assembled to create 3D renderings of each cell type. Approximate blocks of dimensions $20 \times 20 \times 10$ µm were imaged and visualized using FIB-SEM, and the images were used to create a 3D rendering with ImageJ. (a) Seed aleurone cells, (b) stem cortex, (c) root cortex, (d) leaf mesophyll, (e) petal mesophyll. Abbreviations: Aa = amorphous aggregrate; Ap = amyloplast; Cp = chloroplast; CW = cell wall; ER = endoplasmic reticulum; LB = lipid body; PB = protein body; V = vacuole.

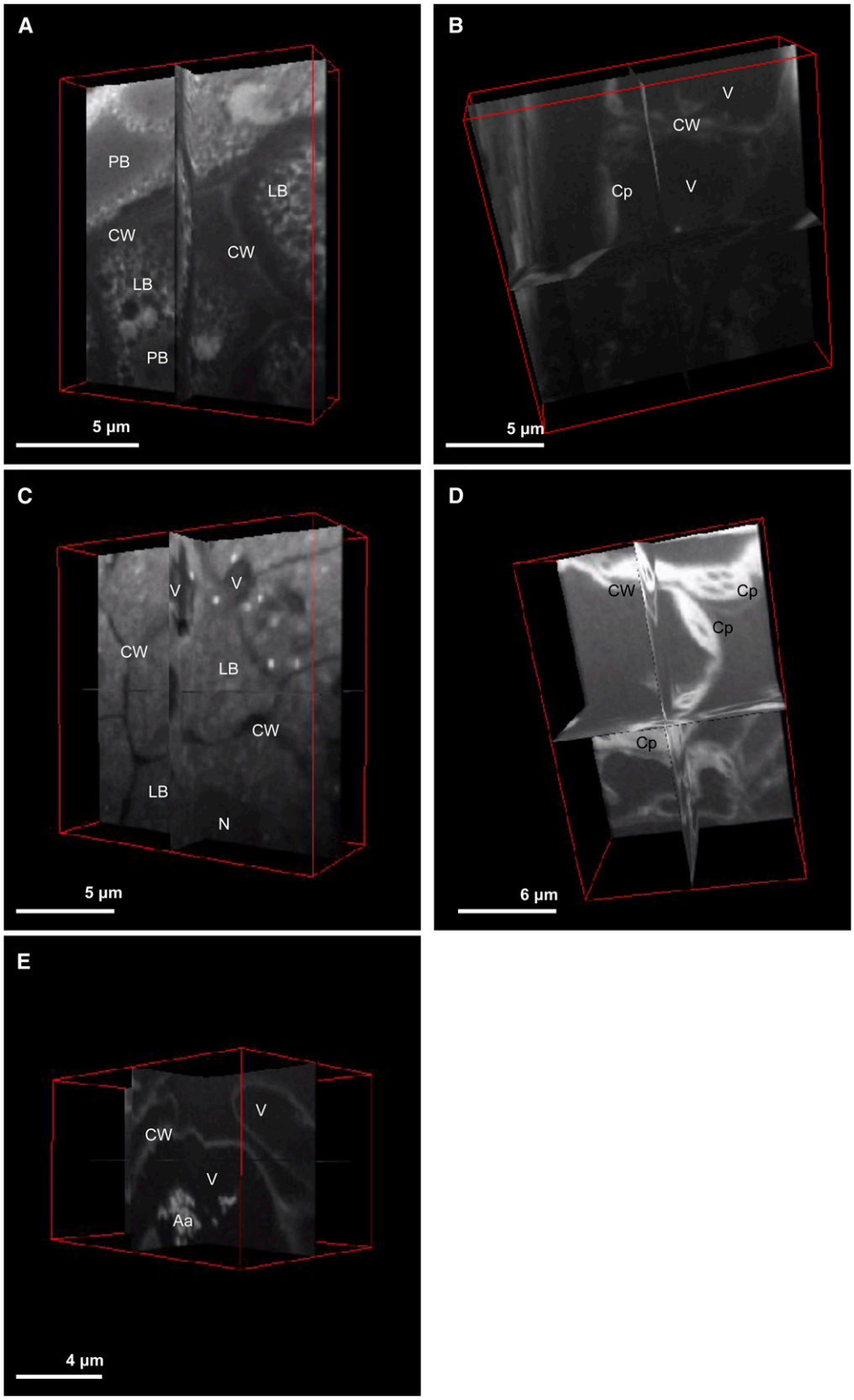

Fig. 4. 360° ortho-rotation for the five tissues. 360° ortho-rotations were created to demonstrate the ability to visualize interior planar sections from the 3D reconstructions. (a) Seed aleurone cells, (b) stem cortex, (c) root cortex, (d) leaf mesophyll, (e) petal mesophyll. Abbreviations: Aa = amorphous aggregrate; Cp = chloroplast; CW = cell wall; LB = lipid body; PB = protein body; V = vacuole.

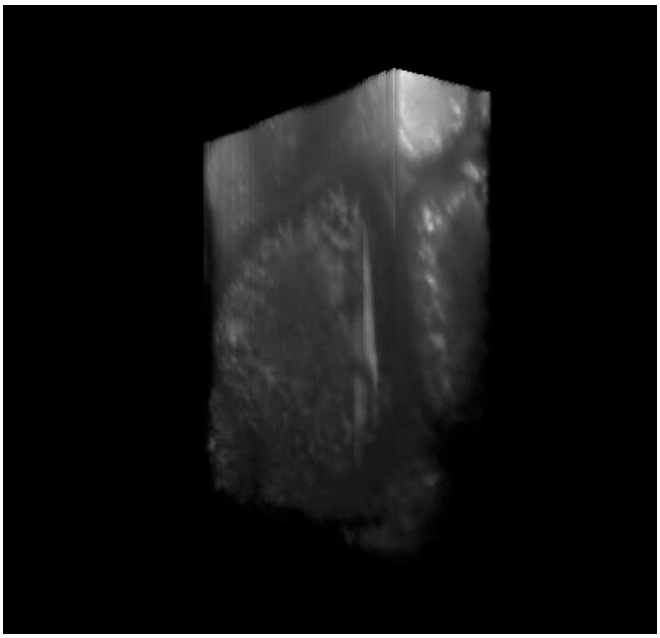

Video 1. 3D reconstruction and rotation of seed endosperm cells from (a) the aleurone layer, (b) stem parenchymal cells, (c) root cortex cells, (d) leaf mesophyll cells, and (e) petal mesophyll cells. Micrographs were collected by milling fixed tissue accompanied by SEM imaging using FIB-SEM. This video is Windows Media (.wmv) file and can be viewed here with QuickTime or Windows Media Player, or can be viewed from the Botanical Society of America's YouTube channel.

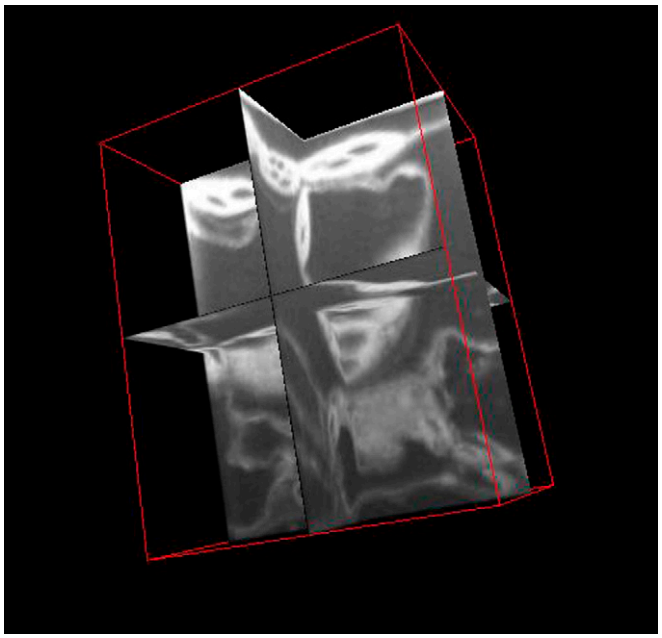

Video 2. 3D ortho-rotation of seed endosperm cells from (a) the aleurone layer, (b) stem parenchymal cells, (c) root cortex cells, (d) leaf mesophyll cells, and (e) petal mesophyll cells. Micrographs were collected by milling fixed tissue accompanied by SEM imaging using FIB-SEM. This video is Windows Media (.wmv) file and can be viewed here with QuickTime or Windows Media Player, or can be viewed from the Botanical Society of America's YouTube channel.

have greatly decreased the labor necessary to produce images and have increased the range of applications. For example, X-ray tomography allows imaging of whole plant organs (Mairhofer et al., 2012), and TEM tomography allows the detailed visualization of subcellular structures (Austin and Staehelin, 2011). FIB-SEM enables imaging of structures between the resolution capabilities of TEM and X-ray tomographies. It has proven useful in plant studies for the visualization and distribution of starch grains (Crumpton-Taylor et al., 2012) and pollen anatomy (House and Balkwill, 2013). The goal of this study was to modify FIB-SEM protocols developed for animal tissues, determine the efficacy of FIB- SEM in plant tissue and/or cellular studies, and demonstrate its usefulness in studying organelle architecture and distribution. A successful survey of five plant tissues was completed using the modified protocol, and 3D reconstructions were produced that provided visualization of plant cells at a unique resolution.

In the seed aleurone layer, 2D micrographs and a 3D reconstruction of the aleurone cells revealed irregularly shaped cells with densely packed cytoplasm. There were numerous protein bodies and lipid bodies, and well-defined cell walls were easily identifiable and comparable to organelle images in micrographs from TEM studies on endosperm and embryo cells of *Daucus carota* L. seed (Dawidowicz-Grzegorzewska, 1997) and perisperm and endosperm of *Phelipanche aegyptiaca* (Pers.) Pomel seed (Joel et al., 2012).

Stem 2D micrographs and 3D renderings of fixed stem tissue revealed highly vacuolated elongated collenchyma cells with fully developed chloroplasts and starch grains very similar to those seen in micrographs of leaf blades of *Arabidopsis* (Musgrave et al., 1998). Amyloplasts and the cell walls were also identifiable and comparable to those in micrographs of meristem cells in *D. carota* embryo (Dawidowicz-Grzegorzewska, 1997) and endosperm cells of *Arundo formosana* Hack. (Jane, 1999).

Root micrographs and 3D reconstruction of root cells revealed columns of regular block-shaped cells with dense cytoplasm, a prominent nucleus, nucleolus, cell wall, and vacuoles. Subcellular structures were identifiable and comparable to those in published micrographs for *Glycine max* (L.) Merr. root cells (Yu et al., 2011) and cortical cells of *Cucumis sativus* L. root (Lee et al., 2002). Lipid bodies and starch grains were identifiable and comparable to those seen in micrographs for *A. formosana* endosperm cells (Jane, 1999) and *D. carota* (Dawidowicz-Grzegorzewska, 1997). Membranes adjacent to the nucleus and throughout the cells were similar to endoplasmic reticulum found in root meristematic cells of *Allium sativum* L. (Jiang and Liu, 2010) and cortical cells of *C. sativus* root (Lee et al., 2002).

Leaf 2D images and 3D renderings of fixed leaf mesophyll cells produced by FIB-SEM allowed the visualization of cellular and subcellular features and provided a view of chloroplast distribution that was unique, but also consistent with previously published 2D electron micrographs (Musgrave et al., 1998). Cell shape was generally oblate and circular, with relatively thin cell walls. Chloroplasts with low-resolution thylakoid stacks were also clearly identifiable as were nuclei, starch grains, and internal cytoplasmic membranes.

Petal mesophyll 2D images and 3D renderings revealed elongated, irregularly shaped cells arranged into aerenchymous tissue as previously reported for *Arabidopsis* (Pyke and Page, 1998) and numerous other species (Kay et al., 1981). Cells were

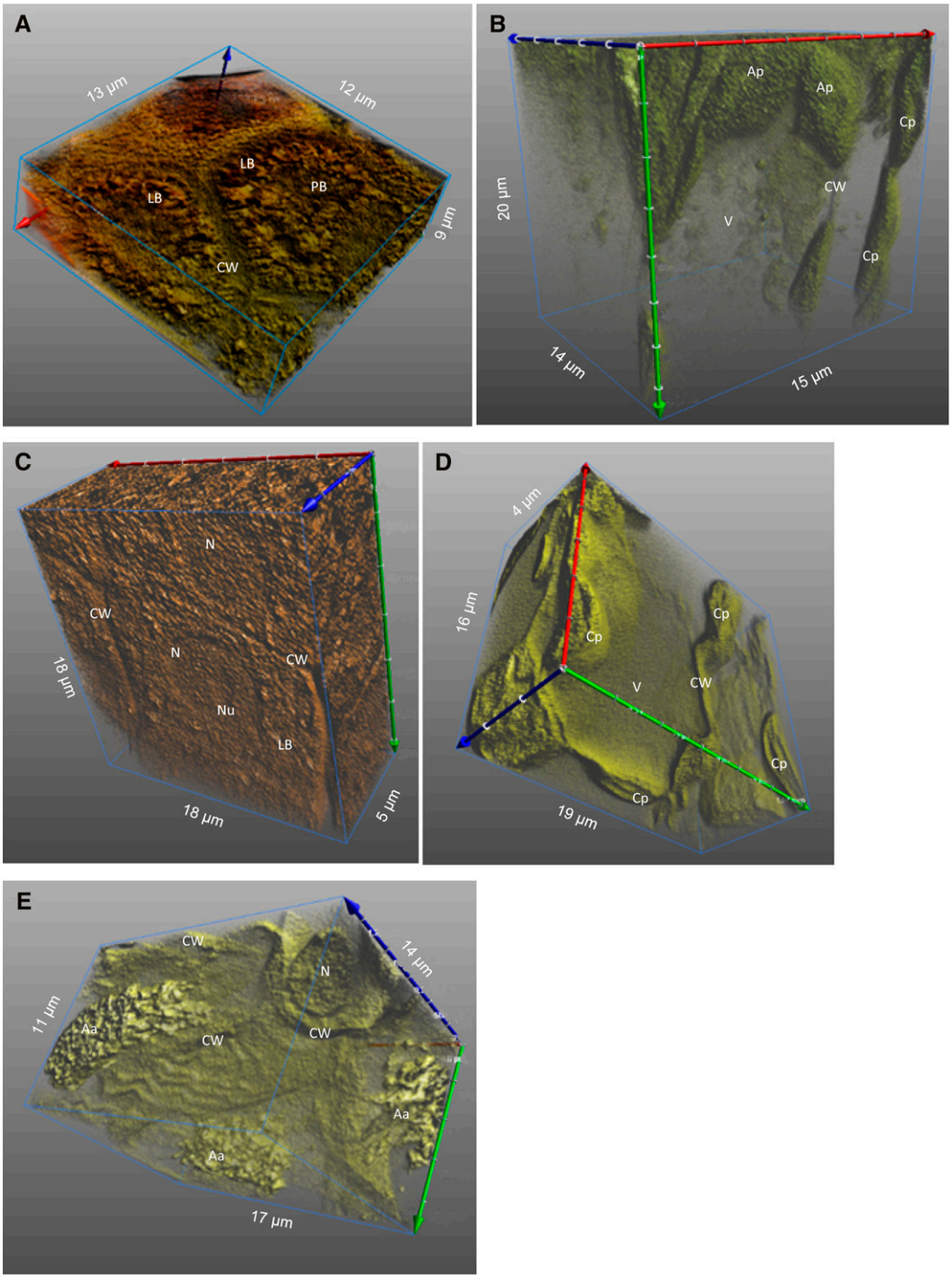

Fig. 5. 3D false-colored volume rendering for the five cell types. False-coloring was manually added to 3D reconstructions to add greater contrast to some of the prominent structures. (a) Seed aleurone cells, (b) stem cortex to parenchymal cells, (c) root endodermis to cortex cells, (d) leaf mesophyll cells, (e) petal mesophyll cells. Axes are color coded: x = red, y = green, z = blue. Abbreviations: Aa = amorphous aggregrate; Ap = amyloplast; Cp = chloroplast; CW = cell wall; LB = lipid body; N = nucleus; Nu = nucleolus; PB = protein body; V = vacuole.

highly vacuolated similar to those of another member of the Brassicaceae, *Erysimum cheiri* (L.) Crantz (Weston and Pyke, 1999). Published transmission electron micrographs of *Arabidopsis* white petal mesophyll have shown electron-dense leucoplasts in the thin strip of cytoplasm typical for these cells (Pyke and Page, 1998). There were several structures that may have been mitochondria, leucoplasts, or large vesicles, but the SEM images obtained in this study lacked the resolution to definitively identify them. Inside the petal mesophyll cell vacuoles, an amorphous aggregate was clearly visible in 3D reconstructions. This feature has been mentioned in 2D TEM studies as an electron opaque material in the mesophyll and epidermal cell vacuoles

of *Erysimum* petals (Weston and Pyke, 1999), but its presence in those images was relatively unremarkable.

LITERATURE CITED

Armer, H. E. J., G. Mariggi, K. M. Y. Png, C. Genoud, A. G. Monteith, A. J. Bushby, H. Gerhardt, and L. M. Collinson. 2009. Imaging transient blood vessel fusion events in Zebrafish by correlative volume electron microscopy. *PLoS ONE* 4: e7716.

Austin, J. R., and L. A. Staehelin. 2011. Three-dimensional architecture of grana and stroma thylakoids of higher plants as determined by electron tomography. *Plant Physiology* 155: 1601–1611.

Bushby, A. J., K. M. Y. P'ng, R. D. Young, C. Pinali, C. Knupp, and A. J. Quantock. 2011. Imaging three-dimensional tissue architectures by focused ion beam scanning electron microscopy. *Nature Protocols* 6: 845–858.

Crumpton-Taylor, M., S. Grandison, K. M. Y. Png, A. J. Bushby, and A. M. Smith. 2012. Control of starch granule numbers in *Arabidopsis* chloroplasts. *Plant Physiology* 158: 905–916.

Dawidowicz-Grzegorzewska, A. 1997. Ultrastructure of carrot seeds during matriconditioning with Micro-Cel E. *Annals of Botany* 79: 535–545.

De Winter, D. A. M., C. T. W. M. Schneijdenberg, M. N. Lebbink, B. Lich, A. J. Verkleij, M. R. Drury, and B. M. Humbel. 2009. Tomography of insulating biological and geological materials using focused ion beam (FIB) sectioning and low-kV BSE imaging. *Journal of Microscopy* 233: 372–383.

Drobne, D., M. Milani, V. Lešer, F. Tatti, A. Zrimec, N. Žnidaršic, R. Kostanjšek, and J. Štrus. 2008. Imaging of intracellular spherical lamellar structures and tissue gross morphology by a focused ion beam/scanning electron microscope (FIB/SEM). *Ultramicroscopy* 108: 663–670.

Giannuzzi, L. A. 2005. Introduction to focused ion beams: Instrumentation, theory, techniques and practice. Springer, New York, New York, USA.

Giannuzzi, L. A., B. W. Kempshall, S. M. Schwarz, J. K. Lomness, B. I. Prenitzer, and F. A. Stevie. 2005. FIB lift-out specimen preparation techniques. *In* L. A. Giannuzzi and F.A. Stevie [eds.], Introduction to focused ion beams, 201–228. Springer, New York, New York, USA.

Hekking, L. H. P., M. N. Lebbink, D. A. M. De Winter, C. T. W. M. Schneijdenberg, C. M. Brand, B. M. Humbel, A. J. Verkleij, and J. A. Post. 2009. Focused ion beam-scanning electron microscope: Exploring large volumes of atherosclerotic tissue. *Journal of Microscopy* 235: 336–347.

Helmstaedter, M., K. L. Briggman, and W. Denk. 2008. 3D structural imaging of the brain with photons and electrons. *Current Opinion in Neurobiology* 18: 633–641.

Heymann, J. A. W., M. Hayles, I. Gestmann, L. A. Giannuzzi, B. Lich, and S. Subramaniam. 2006. Site-specific 3D imaging of cells and tissues with a dual beam microscope. *Journal of Structural Biology* 155: 63–73.

House, A., and K. Balkwill. 2013. FIB-SEM: An additional technique for investigating internal structure of pollen walls. *Microscopy and Microanalysis* 19: 1535–1541.

Jane, W. 1999. Ultrastructure of embryo development in *Arundo formosana* Hack. (Poaceae). *International Journal of Plant Sciences* 160: 46–63.

Jiang, W., and D. Liu. 2010. Pb-induced cellular defense system in the root meristematic cells of *Allium sativum* L. *BMC Plant Biology* 10: 40.

Joel, D. M., H. Bar, A. M. Mayer, D. Plakhine, H. Ziadne, J. H. Westwood, and G. E. Welbaum. 2012. Seed ultrastructure and water absorption pathway of the root-parasitic plant *Phelipanche aegyptiaca* (Orobanchaceae). *Annals of Botany* 109: 181–195.

Kay, Q. O. N., H. S. Daoud, and C. H. Stirton. 1981. Pigment distribution, light reflection and cell structure in petals. *Botanical Journal of the Linnean Society* 83: 57–83.

Knott, G., H. Marchman, D. Wall, and B. Lich. 2008. Serial section scanning electron microscopy of adult brain tissue using focused ion beam milling. *Journal of Neuroscience* 28: 2959–2964.

Knott, G., S. Rosset, and M. Cantoni. 2011. Focused ion beam milling and scanning electron microscopy of brain tissue. *Journal of Visualized Experiments* 53: 2588.

Lee, S. H., A. P. Singh, G. C. Chung, Y. S. Kim, and I. B. Kong. 2002. Chilling root temperature causes rapid ultrastructural changes in cortical cells of cucumber (*Cucumis sativus* L.) root tips. *Journal of Experimental Botany* 53: 2225–2237.

Lehrer, J. 2009. Neuroscience: Making connections. *NATNews* 457: 524–527.

Mairhofer, S., S. Zappala, S. R. Tracy, C. Sturrock, M. Bennett, S. J. Mooney, and T. Pridmore. 2012. RooTrak: Automated recovery of three-dimensional plant root architecture in soil from X-ray microcomputed tomography images using visual tracking. *Plant Physiology* 158: 561–569.

Marko, M., C. Hsieh, R. Schalek, J. Frank, and C. Mannella. 2007. Focused-ion-beam thinning of frozen-hydrated biological specimens for cryo-electron microscopy. *Nature Methods* 4: 215–217.

Merchán-Pérez, A., J.-R. Rodriguez, L. Alonso-Nanclares, A. Schertel, and J. DeFelipe. 2009. Counting synapses using FIB/SEM microscopy: A true revolution for ultrastructural volume reconstruction. *Frontiers in Neuroanatomy* 3: 18.

Micheva, K. D., and S. J. Smith. 2007. Array tomography: A new tool for imaging the molecular architecture and ultrastructure of neural circuits. *Neuron* 55: 25–36.

Mikuła, A., T. Tykarska, M. Zielińska, M. Kuraś, and J. J. Rybczyński. 2004. Ultrastructural changes in zygotic embryos of *Gentiana punctata* L. during callus formation and somatic embryogenesis. *Acta Biologica Cracoviensia. Series Botanica* 46: 109–120.

Murashige, T., and F. Skoog. 1962. A revised medium for rapid growth and bio assays with tobacco tissue cultures. *Physiologia Plantarum* 15: 473–497.

Musgrave, M. E., A. Kuang, C. S. Brown, and S. W. Matthews. 1998. Changes in *Arabidopsis* leaf ultrastructure, chlorophyll and carbohydrate content during spaceflight depend on ventilation. *Annals of Botany* 81: 503–512.

Pellegrini, M. 1980. Three-dimensional reconstruction of organelles in *Euglena gracilis* Z. I. Qualitative and quantitative changes of chloroplasts and mitochondrial reticulum in synchronous photoautotrophic culture. *Journal of Cell Science* 43: 137–166.

Pyke, K. A., and A. M. Page. 1998. Plastid ontogeny during petal development in *Arabidopsis. Plant Physiology* 116: 797–803.

Schneider, C. A., W. S. Rasband, and K. W. Eliceiri. 2012. NIH Image to ImageJ: 25 years of image analysis. *Nature Methods* 9: 671–675.

Schneider, G., P. Guttmann, S. Heim, S. Rehbein, F. Mueller, K. Nagashima, J. B. Heymann, et al. 2010. Three-dimensional cellular ultrastructure resolved by X-ray microscopy. *Nature Methods* 7: 985–987.

Sugiyama, M., and G. Sigesato. 2004. A review of focused ion beam technology and its applications in transmission electron microscopy. *Journal of Electron Microscopy* 53: 527–536.

Tanaka, K., and A. Mitsushima. 1984. A preparation method for observing intracellular structures by scanning electron microscopy. *Journal of Microscopy* 133: 213–222.

Wei, D., S. Jacobs, S. Modla, S. Zhang, C. L. Young, R. Cirino, J. Caplan, and K. Czymmek. 2012. High-resolution three-dimensional reconstruction of a whole yeast cell using focused-ion beam scanning electron microscopy. *BioTechniques* 53: 41–48.

Weston, E. L., and K. A. Pyke. 1999. Developmental ultrastructure of cells and plastids in the petals of wallflower (*Erysimum cheiri*). *Annals of Botany* 84: 763–769.

Yu, H. N., P. Liu, Z. Y. Wang, W. R. Chen, and G. D. Xu. 2011. The effect of aluminum treatments on the root growth and cell ultrastructure of two soybean genotypes. *Crop Protection (Guildford, Surrey)* 30: 323–328.